Study on Rotor Current Waveforms in an Inverter-fed Induction Motor Drive During Overmodulation

V. S. S. Pavan Kumar Hari and G. Narayanan

***Abstract*—Overmodulation introduces low-order harmonics in the output voltage of a voltage source inverter. This paper presents the effects of low-order harmonics in the stator voltage on the rotor currents of an induction motor. Rotor current waveforms are presented for various operating zones in overmodulation, including six-step mode. Harmonic spectra of stator and rotor currents are compared in six-step mode of operation. Pulsating torque is evaluated at various depths of modulation during overmodulation.**

***Index Terms*—Induction motor drives, low-order harmonics, overmodulation, rotor current.**

I. Introduction

VOLTAGE source inverters (VSI) are conventionally used in variable speed induction motor drive applications. Pulse width modulation (PWM) is employed to achieve a voltage of variable magnitude and variable frequency from VSI with a fixed DC bus voltage V_{DC}. A VSI is shown schematically in Fig. 1. Triangle-comparison based approach

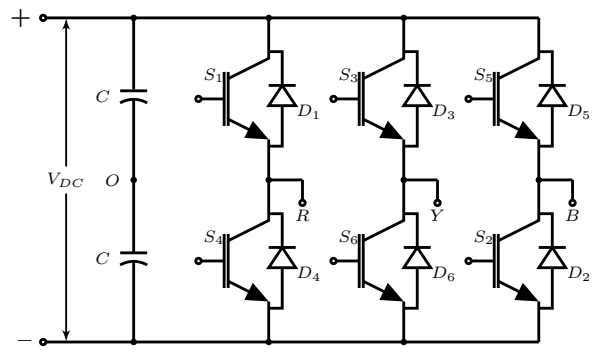

Fig. 1. Two level voltage source inverter using insulated gate bipolar transistors.

is the most popular method of generating PWM waveforms for a VSI. A well-known PWM technique in this approach is the sine-triangle PWM (SPWM), wherein three-phase sinusoidal modulating waves are compared against a common triangular carrier to generate the PWM pulses for the three phases of a VSI. The fundamental component of each phase voltage is proportional to the corresponding sinusoidal reference, for a given V_{DC} with the peak of the reference sine wave (V_m) being less than or equal to the peak of the triangle (V_p). The ratio $\frac{V_m}{V_p}$ is referred to as *modulation index* m. When $m \leq 1$, the mode of operation is called "linear modulation". The maximum peak value of fundamental phase voltage with SPWM in linear modulation is $0.5V_{DC}$ [1]-[3].

Addition of third harmonic to the three-phase references increases the highest possible AC output voltage for a given V_{DC}. This technique is known as third harmonic injection PWM (THIPWM). The peak value of fundamental phase voltage can be increased upto $0.577V_{DC}$ using THIPWM in linear modulation [2]-[3].

To obtain any peak phase fundamental voltage which is greater than $0.577V_{DC}$, the VSI must be operated in overmodulation. The limit of overmodulation is the square-wave mode or six-step mode of operating VSI. The maximum possible peak phase voltage from a VSI with fixed V_{DC} is obtained in six-step mode, which equals $2\frac{V_{DC}}{\pi}$ [3].

The output voltage of VSI has fundamental component at the frequency of modulating wave (f_m). In addition, it contains harmonics around the frequency of carrier wave (f_c) and its integral multiples. However, in induction motor drives, the leakage inductance of the motor is sufficient to filter out the harmonics at f_c and its multiples, when f_c is chosen to be much higher than f_m [3]. The motor current waveform is "nearly" sinusoidal.

Overmodulation introduces additional harmonics in the output voltage of a VSI at $5f_m$, $7f_m$, $11f_m$, $13f_m$ and so on. These are called low-order harmonics, which increase the distortion in the output voltage of a VSI. The low-order harmonic voltages cause corresponding harmonic currents to flow in the stator windings, thereby inducing voltages other than slip frequency in rotor phases. Thus, the rotor phases carry harmonic currents which interact with fundamental air gap flux, leading to torque pulsations [4]. Further, the harmonic currents result in increased copper losses in the motor [5]. This paper shows experimentally-observed rotor currents when the stator is fed with low-order harmonics. This work is a preliminary step towards understanding the effects of stator-side harmonics on rotor and vice versa. Such a study would be helpful in predicting the performance of a slip ring induction motor with non-sinusoidal voltages being impressed on stator as well as rotor. This could lead to the development of pulse width modulation strategies for a double VSI fed slip ring induction motor drive.

V. S. S. Pavan Kumar Hari and G. Narayanan are with Department of Electrical Engineering, Indian Institute of Science, Bangalore 560012, India (e-mail: pavan@ee.iisc.ernet.in; gnar@ee.iisc.ernet.in).

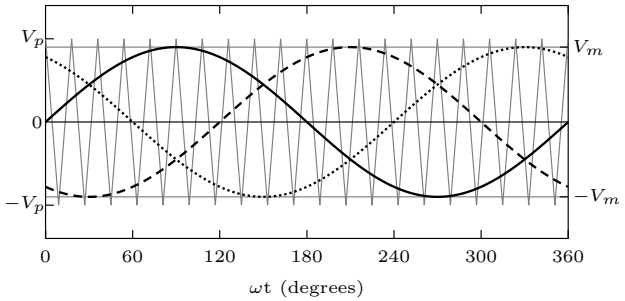

(a) Linear modulation ($m = 0.9$)

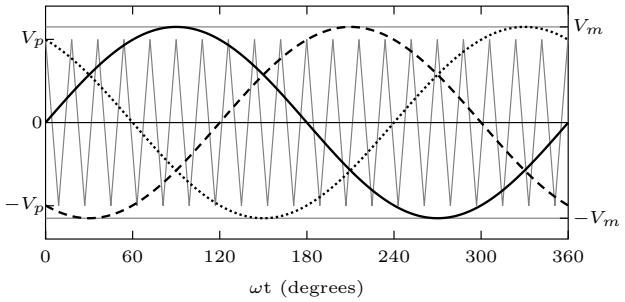

(b) Overmodulation($m = \frac{2}{\sqrt{3}}$)

Fig. 2. Sine-triangle PWM : Linear modulation and overmodulation.

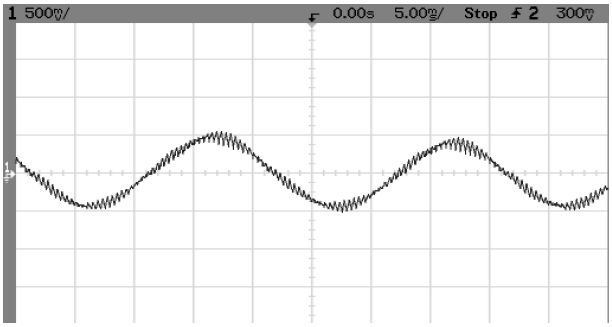

(a) Stator Current

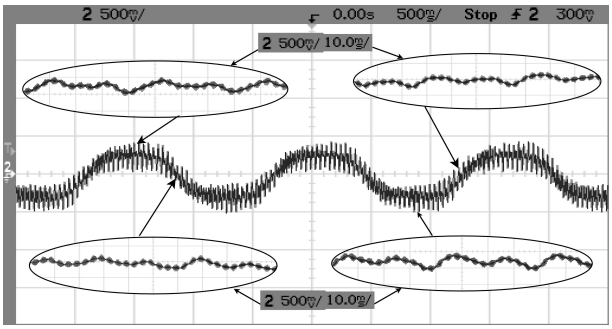

(b) Rotor Current

Fig. 3. Measured stator and rotor current waveforms in linear modulation on no-load. Modulation index=0.9 and Carrier frequency=2.5kHz.

II. Overmodulation

This section presents a brief review of overmodulation in sine-triangle comparison based approach.

Three-phase sinusoidal modulating waves and a high frequency triangular carrier are shown in Fig. 2. The peak value of modulating waves is always less than the peak of triangular wave in linear modulation. An example of linear modulation is shown in Fig. 2(a), where $m = 0.9$. The AC output terminals R, Y and B of a VSI are called poles (see Fig. 1). The voltage between a pole and the mid-point of DC bus O is termed as *pole voltage*. Assuming that the modulating waves are sampled at each carrier-peak, the average value of the pole voltage over a half-carrier cycle is proportional to the value of modulating wave. Thus, the average pole voltage varies sinusoidally over a fundamental cycle and is equal to the fundamental component of the phase to neutral voltage, when the VSI is feeding the stator of an induction motor with isolated neutral.

Increasing the value of V_m beyond V_p disturbs the linear relation between modulating wave and output phase voltage, which is known as overmodulation. One or more of the phases get clamped to either positive or negative DC bus when $|V_m| > |V_p|$. Thus, the average pole voltage does not vary sinusoidally and low-order harmonics such as 5^{th}, 7^{th}, 11^{th} and 13^{th} begin to appear in the voltage applied on the motor.

Overmodulation is characterized by pulse-dropping [6]. The overmoduation zone can be divided into three sub-zones A, B and C in terms of the number of phases which experience pulse-dropping concurrently. For $1 < m < \frac{2}{\sqrt{3}}$, the number of phases that experience pulse-dropping is 0 or 1 in any given carrier cycle. This sub-zone is referred to as region A. The limiting condition for region A is $m = \frac{2}{\sqrt{3}}$, where pulse-dropping occurs in one of the phases throughout the fundamental cycle [6]. This condition is shown in Fig. 2(b).

For $\frac{2}{\sqrt{3}} < m < 2$, at least one and a maximum of two phases experience pulse-dropping concurrently. When $m = 2$, pulse-dropping is experienced concurrently by two phases in any given carrier cycle. This zone of overmodulation is referred to as region B [6]. For $m > 2$, pulse-dropping occurs in at least two phases at any given instant in the fundamental cycle, which is referred to as region C [6]. All the three phases experience pulse-dropping concurrently throughout the fundamental cycle as $m \to \infty$, where the average pole voltage becomes a square-wave. This condition is known as six-step operation.

The magnitude of low-order harmonics increases with modulation index in overmodulation zone. The effect of these harmonics is clearly seen in stator and rotor currents, which are presented in the next section.

III. Experimental Results

The overmodulation algorithm in sine-triangle approach is implemented on *ALTERA Cyclone* based field programmable gate array (FPGA) device [7]. Three-phase sinusoidal modulating functions are generated using CORDIC algorithm avoiding the use of look-up table [8]. The experimental set-up consists of a 10kVA IGBT-based two-level VSI and a 3kW, 415V, 50Hz, 4-pole, 3-Phase slip ring induction motor (SRIM), coupled to a 5.6kW, 220V separately-excited DC generator. Both stator and rotor windings are rated for 415V, with a turns ratio of unity. The VSI is connected to the stator; the rotor terminals are short-circuited. Hall-effect based current sensors are arranged in the rotor circuit to measure the rotor

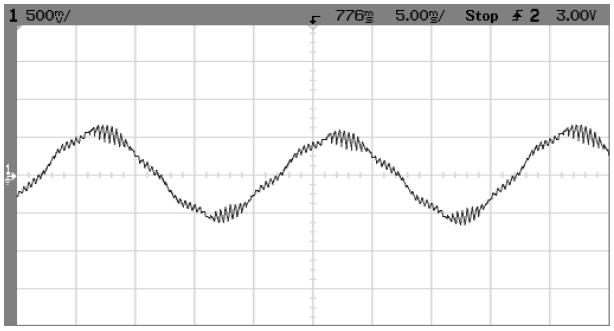

(a) Stator Current

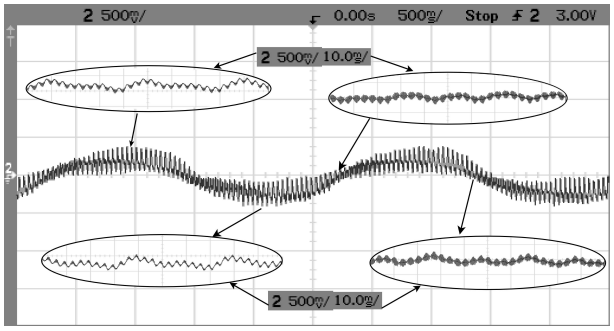

(b) Rotor Current

Fig. 4. Measured stator and rotor current waveforms in overmodulation region B on no-load. Modulation index=1.8 and Carrier frequency=2.5kHz.

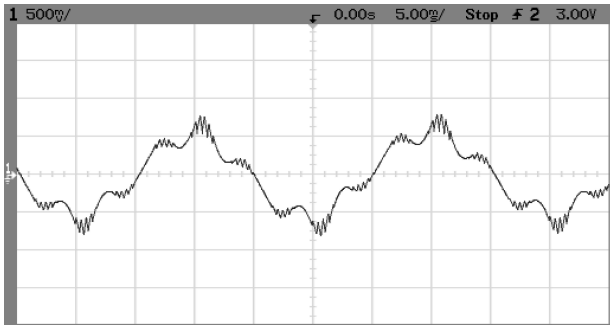

(a) Stator Current

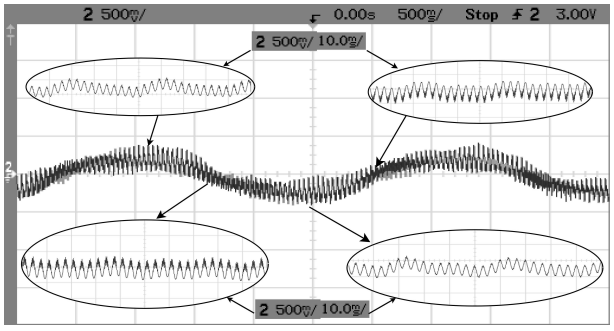

(b) Rotor Current

Fig. 5. Measured stator and rotor current waveforms in overmodulation region C on no-load. Modulation index=3 and Carrier frequency=2.5kHz.

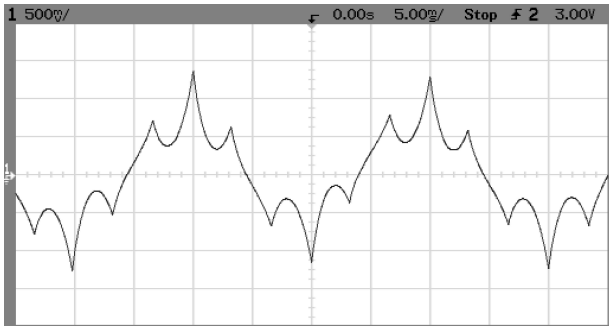

(a) Stator Current

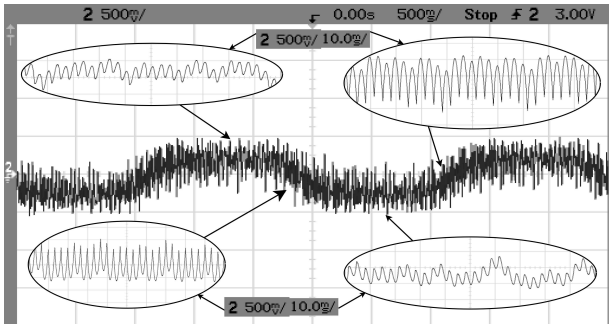

(b) Rotor Current

Fig. 6. Measured stator and rotor current waveforms on no-load during six-step operation.

currents. The DC bus voltage is chosen to be 420V to limit the current peaks in six-step mode.

A. Currents in stator and rotor

Measured no-load stator and rotor current waveforms in linear modulation ($m = 0.9$), overmodulation ($m = 1.8$ and 3) and six-step mode are presented in Fig. 3 to Fig. 6.

When the stator is supplied with three-phase balanced sinusoidal voltages of frequency f, voltages are induced in the rotor windings at slip frequency sf, where s is the slip of the motor. At stand still, $s = 1$; the value of s decreases as the rotor speed increases. Slip has the least value when the motor is on no-load. Thus, the fundamental component of rotor current is at slip frequency sf when the fundamental component of stator voltage is at f. In this experimental set-up, the machine is operated on no-load and the rotor speed is measured to be 1487 rpm. The slip speed is 13 rpm and $s = 0.0087$. The fundamental component of stator voltage is at 50Hz and the fundamental component of rotor current is around 0.5Hz, as can be seen from Fig. 3 to Fig. 6.

If the voltage applied at the stator terminals contains 5^{th} harmonic ($5f$), a corresponding voltage will be induced in the rotor phases at $(5f + f - sf)$ as the 5^{th} harmonic has a phase sequence opposite to that of the fundamental. On the other hand, if the stator voltage contains 7^{th} harmonic ($7f$), the corresponding rotor induced voltage will be at $(7f - f + sf)$ since the 7^{th} harmonic has the same phase sequence as that of the fundamental. In general, if the stator voltage harmonics are of the form $(6n - 1)f$, the corresponding induced voltage harmonics in rotor will be of the form $(6n + s)f$, where $n = 1, 2, 3, ...$ Similarly, voltage harmonics of the

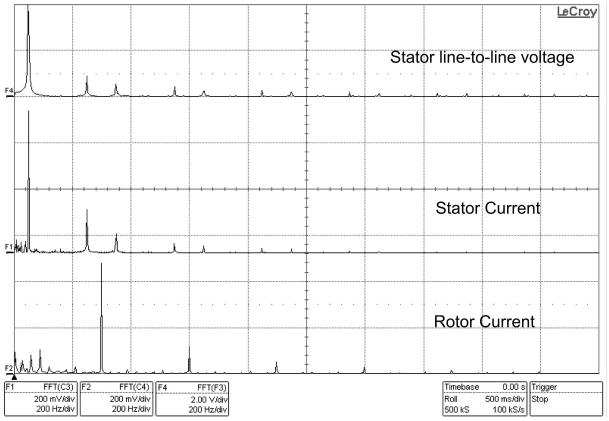

Fig. 7. FFT of stator line-to-line voltage, stator current and rotor current under six-step operation.

form $(6n - s)f$ will be induced in the rotor if the stator voltage contains harmonics of the form $(6n + 1)f$. The slip frequency sf is very small when compared to the fundamental frequency. Hence, the harmonics in rotor induced voltage can be approximated as $6nf$ when the stator is fed by voltage harmonics of the form $(6n \pm 1)f$. The currents in stator and rotor will have harmonics corresponding to the voltage applied and the voltage induced, respectively.

Fig. 4 and Fig. 5 show the stator and rotor currents in overmodulation regions B ($m = 1.8$) and C ($m = 3$), respectively. The slip frequency component is clearly visible in the rotor currents in Fig. 4(b) and Fi. 5(b). Since the dominant harmonic components are at 250Hz and 350Hz in the stator voltage, the dominant harmonic in rotor current is at 300Hz as seen from the figures. The magnitude of 6^{th} harmonic ripple current increases with increasing modulation index as seen from Fig. 4 to Fig. 6. Further, switching-frequency harmonic components can also be observed in the rotor current waveforms. The magnitude of this high frequency component reduces as the operation approaches the six-step mode (on account of pulse-dropping). The 6^{th} harmonic ripple current becomes more dominant when the VSI is operating in six-step mode as shown in Fig. 6. The carrier frequency ripple current vanishes completely in this mode as the switching frequency becomes equal to the fundamental frequency.

B. Harmonic spectra

Fig. 7 shows the measured harmonic spectra of stator line-to-line voltage (R phase PWM minus Y phase PWM), stator current and rotor current under six-step mode. The frequency scale is 200Hz/div. Harmonics of the order $(6n \pm 1)$ can be seen in the stator voltage spectrum. The corresponding stator current spectrum also contains harmonics of the order $(6n \pm 1)$. On the other hand, the rotor current contains harmonics of the order $6n$. The waveforms and spectra corresponding to stator and rotor currents interchange when the rotor is fed by VSI and the stator terminals are short-circuited.

The low-order harmonics introduced by overmodulation cause degradation in the performance of the machine. The machine produces pulsating torque, which is evaluated in the next section.

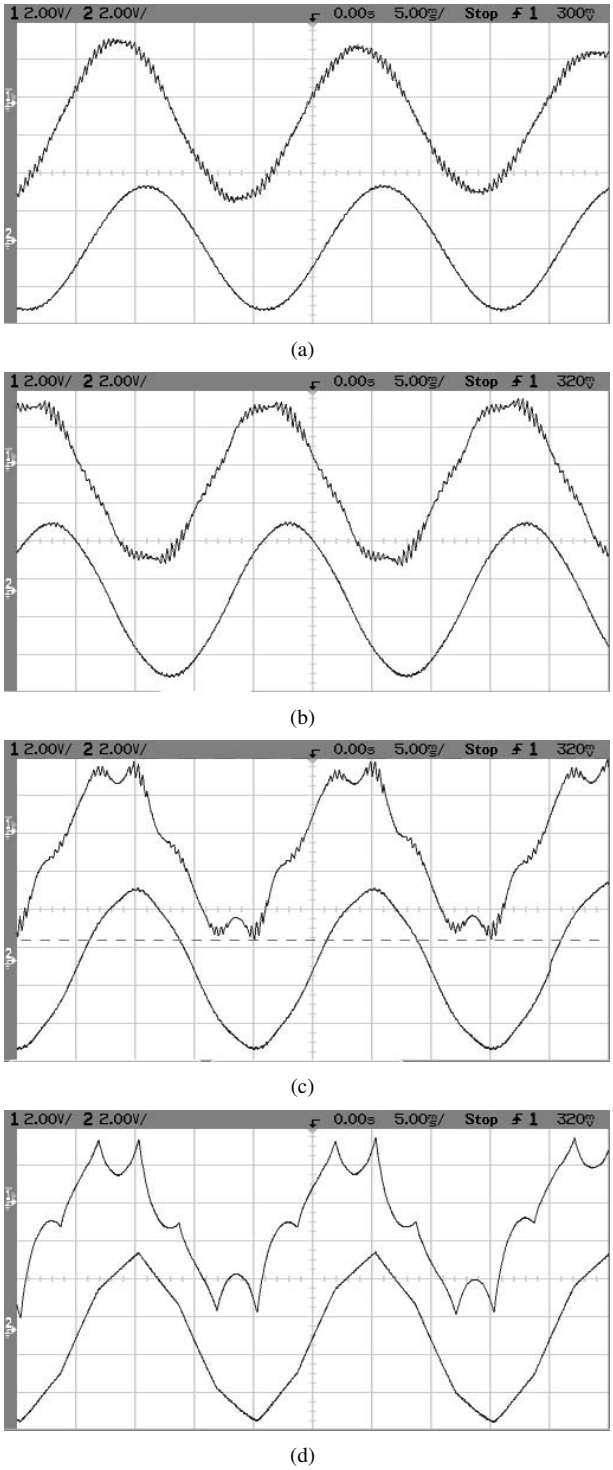

Fig. 8. Waveforms of i_{sa} and ψ_{sa} during (a) Linear modulation (modulation index=0.9), (b) Overmodulation region B (modulation index=1.8), (c) Over-modulation region C (modulation index=3) and (d) six-step operation. The carrier frequency is 2.5kHz and the load on the machine is half the rated load.

IV. Pulsating Torque

Torque developed by an induction machine can be estimated using a standard machine model [9]. Consider two mutually perpendicular axes a and b in the stationary reference frame, where a-axis coincides with the stator R-phase axis of the

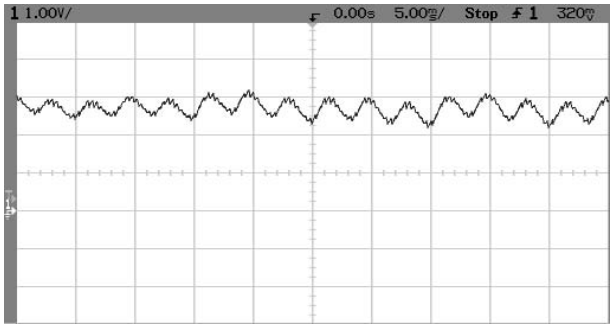

(a)

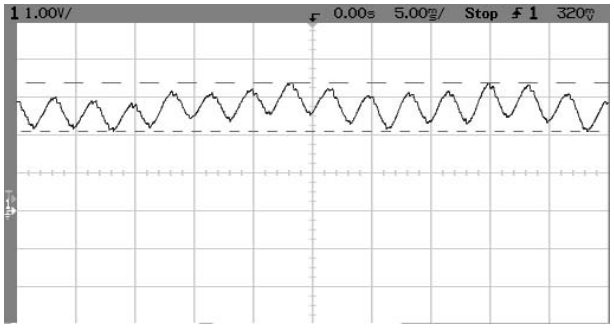

(b)

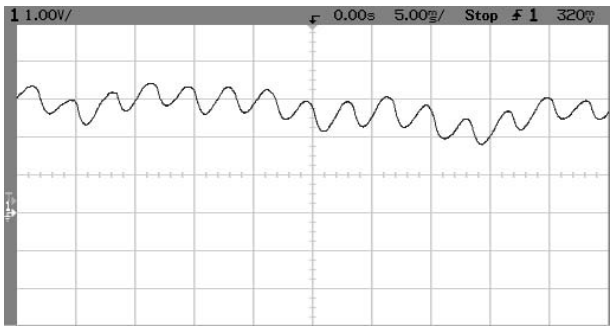

(c)

Fig. 9. Torque developed by the machine during (a) Overmodulation region B (modulation index=1.8), (b) Overmodulation region C (modulation index=3) and (c) six-step operation. The carrier frequency is 2.5kHz and the load on the machine is half the rated load.

machine and b-axis is 90° ahead of the a-axis. The three phase voltages applied to the stator can be transformed to a voltage space vector having components along a and b axes. The components of stator voltage space vector along a and b axes are denoted by v_{sa} and v_{sb}, respectively. The voltages v_{sa} and v_{sb} can be expressed as

$$v_{sa} = v_{RO} - \frac{1}{2}v_{YO} - \frac{1}{2}v_{BO} \quad (1)$$

$$v_{sb} = \frac{\sqrt{3}}{2}\left(v_{YO} - v_{BO}\right) \quad (2)$$

where v_{RO}, v_{YO} and v_{BO} are the three-phase pole voltages respectively (see Fig. 1). The three-phase pole voltages can be obtained by using the three-phase PWM signals and the measured V_{DC}.

The three-phase stator currents measured by current sensors can also be transformed into a space vector having components along a and b axes. If i_{sR}, i_{sY} and i_{sB} are the measured stator currents, the components of stator current space vector along a and b axes are given by [9]

$$i_{sa} = \frac{3}{2}i_{sR} \quad (3)$$

$$i_{sb} = \frac{\sqrt{3}}{2}\left(i_{sY} - i_{sB}\right) \quad (4)$$

The components of the stator flux space vector along a and b axes can be obtained as

$$\psi_{sa} = \int_0^t \left(v_{sa} - i_{sa}R_s\right) d\tau + \psi_{sa}(0) \quad (5)$$

$$\psi_{sb} = \int_0^t \left(v_{sb} - i_{sb}R_s\right) d\tau + \psi_{sb}(0) \quad (6)$$

where R_s is the stator resistance. The instantaneous torque developed by the machine (m_d) can be expressed in terms of stator flux and stator current as given by [9]

$$m_d = \frac{2}{3}\frac{P}{2}\left(\psi_{sa}i_{sb} - \psi_{sb}i_{sa}\right) \quad (7)$$

where P is the number of poles of the machine.

The waveforms of ψ_{sa} and i_{sa} corresponding to $m = 0.9$, $m = 1.8$, $m = 3$ and $m \to \infty$ are shown in Fig. 8(a) to Fig. 8(d), respectively, at half the rated load of the induction motor. The waveforms of ψ_{sb} and i_{sb} (not shown) are phase shifted by 90° with respect to ψ_{sa} and i_{sa}, respectively. The distortion is more prominent in current waveforms than that in the flux waveforms.

The torque developed by the machine under overmodulation and six-step operation of VSI is shown in Fig. 9. Increase in torque ripple due to the low-order harmonics introduced by overmodulation can be observed in Fig. 9(a) and Fig. 9(b). The dominant component in this case is the 6^{th} harmonic torque ripple, which is a result of the interaction between the fundamental flux and the 5^{th} and 7^{th} harmonic rotor currents shown in Fig. 4 and Fig. 5. The torque ripple is maximum under six-step operation as shown in Fig. 9(c).

V. Conclusions

Slip ring induction motor provides an opportunity to study the effects of stator-side harmonics on rotor and *vice versa*. The effects are clearly visible when the harmonics are of low-order as in the case of overmodulation. The pulsating torque is quite prominent during overmodulation and six-step operation. In high power induction motor drives, the switching frequency is quite low and the corresponding harmonics become dominant. Measurement and analysis of rotor current can improve the understanding of torque pulsations and spatial harmonics in induction motor drives.

References

[1] A. Schonung and H. Stemmler,"Static frequency changers with subharmonic control in conjunction with reversible variable speed AC drives", *The Brown Boveri Review*, pp. 555- 577, Sep. 1964.

[2] J. Holtz, "Pulsewidth modulation for electronic power conversion", *Proc. IEEE*, vol. 82(8), pp. 1194-1214, Aug. 1994.

[3] D. G. Holmes and T. A. Lipo, *Pulse width modulation for power converters: Principles and Practice*, Hoboken, NJ: IEEE Press and John Wiley Interscience, 2003.

[4] S. D. T. Robertson and K. M. Hebbar, "Torque pulsations in induction motors with inverter drives", *IEEE Trans. Ind. and Gen. Appl.*, Vol. IGA-7, No. 2, pp. 318-323, Mar./Apr. 1971.
[5] E. A. Klingshirn and H. E. Jordan, "Polyphase Induction Motor Performance and Losses on Nonsinusoidal Voltage Sources", *IEEE Trans. Power App. and Sys.*, Vol. PAS-87, No. 3, pp. 624-631, Mar. 1968.
[6] S. Venugopal, "Study on Overmodulation Methods for PWM Inverter-Fed AC Drives", *M.Sc.(Engg) Thesis*, Indian Institute of Science, Bangalore, May 2006.
[7] S. Venugopal and G. Narayanan, "Design of FPGA based digital platform for control of power electronics systems", *Proc. NPEC '05*, National Power Electronics Conference, Indian Institute of Technology, Kharagpur, Dec. 2005.
[8] J. E. Volder, "The CORDIC Trigonometric Computing technique", *IRE Transactions on Electronic Computers*, pp. 330-334, Sep. 1959.
[9] Werner Leonhard, "Control of Electric Drives", *Springer* International Edition, 2003.